Lasers in Surgery and Medicine 6:494–503 (1987)

Modeling Optical and Thermal Distributions in Tissue During Laser Irradiation

Steven L. Jacques, PhD, and Scott A. Prahl, BS

Department of Dermatology, Massachusetts General Hospital, Harvard Medical School, Boston (S.L.J.); Biomedical Engineering Program, University of Texas, Austin (S.A.P.)

The propagation of light energy in tissues is an important problem in phototherapy, especially with the increased use of lasers as light sources. Often a slight difference in delivered energy separates a useless, efficacious, or disastrous treatment. Methods are presented for experimental characterization of the optical properties of a tissue and computational prediction of the distribution of light energy within a tissue. A standard integrating sphere spectrophotometer measured the total transmission, T_t, total reflectance, R_t, and the on-axis transmission, T_a, for incident collimated light that propagated through the dermis of albino mouse skin, over the visible spectrum. The diffusion approximation solution to the one-dimensional (1-D) optical transport equation computed the expected T_t and R_t for different combinations of absorbance, k, scattering, s, and anisotropy, g, and by iterative comparison of the measured and computed T_t and R_t values converged to the intrinsic tissue parameters. For example, mouse dermis presented optical parameters of 2.8 cm^{-1}, 239 cm^{-1}, and 0.74 for k, s, and g, respectively, at 488 nm wavelength. These values were used in the model to simulate the optical propagation of the 488-nm line of an argon laser through mouse skin in vivo. A 1-D Green's function thermal diffusion model computed the temperature distribution within the tissue at different times during laser irradiation. In vitro experiments showed that the threshold temperature range for coagulation was 60°–70° C, and the kinetics were first order, with a temperature-dependent rate constant that obeyed an Arrhenius relation (molar entropy 276 cal/mol-°K, molar enthalpy 102 kcal/mol). The model simulation agreed with the corresponding in vivo experiment that a 2-s pulse at 55 W/cm^2 irradiance will achieve coagulation of the skin.

Key words: lasers, skin, mice, lasers/tu, light coagulation

INTRODUCTION

The propagation of light within tissues is an important problem that confronts the dosimetry of therapeutic laser delivery and the development of diagnostic spectroscopy. In the clinical application of photodynamic therapy (PDT) and in other research applications in photobiology, the photon deposition within a tissue determines the spatial distribution of photochemical reactions. When high intensities of light are delivered, eg, during laser irradiation, thermal damage is possible, and the photon deposition becomes the distributed heat source for a thermal diffusion problem. We have developed an animal model (albino BALB/c mouse) for the study of cutaneous tissue responses to thermal damage caused by argon laser irradiation, which yields reproducible, even, full thickness aseptic wounds (R. Granstein, S. Jacques, unpublished study). This paper presents 1) the experimental determination of the threshold temperature range and kinetics for coagulation of mouse skin, and 2) the experimental specification of the threshold laser irradiance and exposure duration (488 nm) required for photocoagulation of mouse skin in vivo.

Standard spectrophotometric equipment was used for optical measurements on the thin tissue samples. The simple geometry of the in vitro measurement allowed a three-parameter model to uniquely specify the intrinsic optical parameters of the tissue: scattering (s), absorption (k), and anisotropy (g). These intrinsic tissue parameters become available for other more sophisticated models to predict optical distributions in complex geometries. This paper outlines the procedures that computed 1) the optical parameters, s, k, and g, based on experimental measure-

Address reprint requests to Steven L. Jacques, PhD, Wellman Laboratories, Department of Dermatology, Massachusetts General Hospital, Boston, MA 02114.

Accepted for publication September 17, 1986.

ments, 2) the photon deposition within in vivo mouse skin, and 3) the temporal evolution of the temperature distribution within the skin during simulated laser irradiation by the 488-nm argon laser. The procedures presented offer a general approach toward specification of the intrinsic optical properties of thin tissues.

MATERIALS AND METHODS

Tissue

Fourteen 6–8-week-old BALB/c albino mice were sacrificed in pairs, and the fur was plucked from the back. The full thickness skin was excisd from the back in a 2 × 4-cm rectangular sample. The fat layer was removed by scraping with forceps until only the dermis and the thin epidermis remained. Each sample was immediately placed on a glass slide with the dermis against the glass and the epidermis exposed to the air. The loss of moisture across the stratum corneum was minimal. The exposed edges of a sample dried slightly during the experiment, which retarded further water loss. The edges were not involved in the optical measurements. Each sample thickness was determined by micrometer measurements of the tissue between glass slides of known thickness. After optical measurements were made on each sample, the two samples were placed together to provide a thicker tissue specimen for a third optical measurement. Some manipulation was required to remove air bubbles between the samples, which slightly stretched the samples and reduced the net thickness. Micrometer measurements documented the final thickness of the double layer.

Optical Measurements

A standard integrating sphere spectrophotometer (Beckman UV 5270) was used for optical transmission and reflection measurements, as outlined in Figure 1. The integrating sphere was used to measure the total transmission, T_t, and total reflectance, R_t, from the skin sample mounted on the glass slide. The sample was placed at the entry port of the sphere during measurements of T_t. Collimated light directly struck the sample and propagated into the integrating sphere for detection. During measurements of R_t, the sample was removed from the entry port and replaced a removable $BaSO_4$ plate at the back exit port. Collimated light entered the entry port and directly struck the sample positioned at the back exit port, and reflected light was detected within the sphere. As a supplemental measurement to test the predictive ability of the model, the total reflectance with a black backing, R_0, was measured where the tissue sample rested on the blackened surface of a painted glass slide or on an agar gel containing black India ink. These absorbing boundaries eliminated internal reflectance at the dermis/glass/air interface on the back side of the sample.

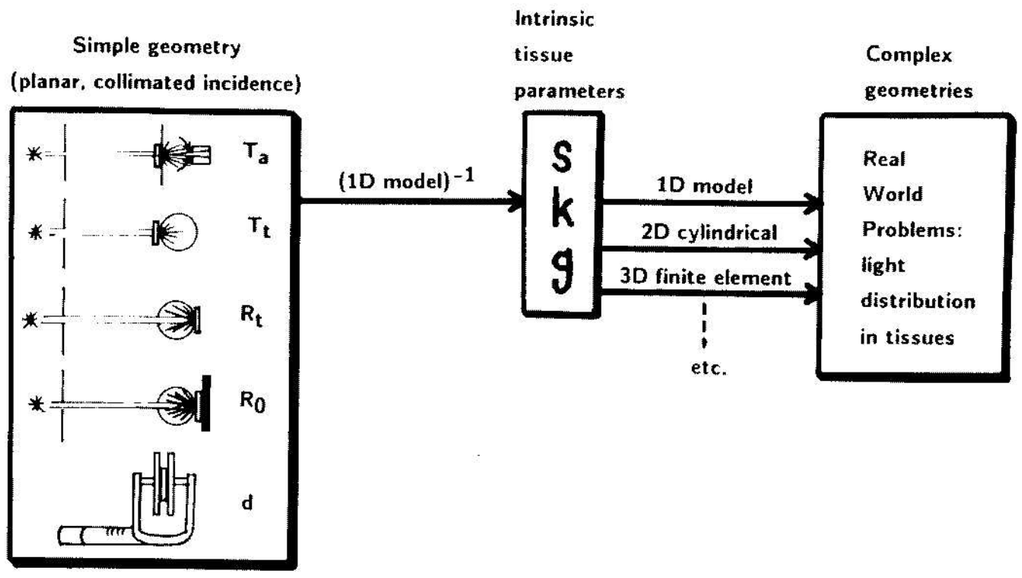

Fig. 1. The optical measurements conducted on mouse dermis. The on-axis transmission, T_a, was made with the standard spectrophotometer configuration. The integrating sphere was used for measurements of total transmission, T_t, total reflection, R_t, and total reflection with a black backing, R_0. The 1-D diffusion approximation solution to the transport equation [Ishimaru, 1978] provided the theoretical model.

Removal of the integrating sphere assembly allowed measurements of the on-axis transmission, T_a, by placement of the sample over the standard exit port. Collimated light struck the sample, but only light that continued to propagate on-axis beyond the sample was detected. To determine the solid angle of collection by the detector, measurements were made on a 2-mm thickness of Teflon, which yielded a perfectly diffuse transmission pattern as verified by angular scattering experiments not presented here. The on-axis transmission, T_a, was 0.08% ± 0.01% (SD for five wavelengths, 486–490 nm). The total transmission, T_t, measured with the integrating sphere was 27.0% ± 0.1%. The ratio T_a/T_t was 0.00296. This ratio is a function of the half-angle, θ, off the central axis for collection of light:

$$T_a/T_t = 1/(2\pi R^2) \int_0^{\theta} 2\pi R \sin(\theta) \cos(\theta)\, R\, d\theta = \frac{\sin^2(\theta)}{2}$$

or

$$\theta = \arcsin([2T_a/T_t]^{1/2}), \quad (1)$$

where the $\cos(\theta)$ term is introduced to account for Lambert's law of cosines [see Sliney and Wolbarsht, 1980], which describes the observation of light from a diffuse planar light source. According to equation 1, the ratio T_a/T_t, 0.00296, corresponds to a 4.4° half-angle θ of collection off the central axis, or 0.039 steradians of solid angle. (The concept of solid angle is valid only for a point source of light, so an approximation is made here when we treat the diffuse light transmitted by the Teflon slab as a point source.)

A portion of the measured T_a is due to diffuse light transmission. The ratio, b, equal to T_a/T_t that was observed for the Teflon slab was 0.00296. Therefore, we assumed that 0.296% of the total transmitted light, T_t, would be collected in the T_a measurement but should not be considered as collimated transmission, T_c. The following relation was used to calculate the measured T_c minus the contribution from T_t:

$$\text{measured } T_c = (T_a - bT_t)/(1 - b) \qquad (2)$$

The ratio T_c/T_a was 0.93 $\pm$ 0.08 over 21 measurements, which indicated that this was a minor correction.

The value for T_c included the effects of specular reflectance, R_s, at discontinuities in refractive index. The R_s is $(n_2-n_1)^2/(n_2+n_1)^2$ between two media with indices of refraction n_1 and n_2. In general, the refractive index of tissue varies between 1.33 and 1.5 for water contents between 100% and 0% [Bausch and Lomb]. The n for dry stratum corneum at the skin surface is about 1.45 [Solan et al, 1977], appropriate for a 30% water content. Therefore, the R_{s1} at the air/epidermis interface was assumed to be 3.4%. This neglected the effects of surface roughness. At the back of the tissue, collimated light encounters a wet dermis/glass/air interface. The n for wet dermis (about 70% water content), glass, and air are 1.38, 1.55, and 1, respectively. Because multiple reflections occur between the tissue/glass and glass/air interfaces, the net reflectance from this interface is given:

$$R_{s2} = 1 - (1 - R_1)(1 - R_2)[1 + \sum_i R_1^i R_2^i] \qquad (3)$$

where R_1 is the dermis/glass reflectance 0.3%, and R_2 is the glass/air reflectance 4.7%. The net R_{s2} is 5.0%. Therefore, the value for T_c, was corrected for specular reflectances:

$$\text{actual } T_c = (\text{measured } T_c)/(1 - R_{s1})(1 - R_{s2}) \qquad (4)$$

In summary, a measured T_a was corrected by equation 2 to account for the contribution from T_t and yield the measured T_c, then equation 4 accounted for specular reflectances to yield the actual T_c.

The observed values T_t and R_t also included the effects of specular reflectance, and were related to the diffuse transmission and reflectance, T_d and R_d, as discussed in Appendix I.

The internal reflectance r_i of diffuse light at the air/epidermis and the dermis/glass/air interfaces must also be considered. Although the front and surfaces should exhibit different values for r_i, the differences were expected to be small, based on an analysis using the Fresnel equations (calculations not shown). The measurements, T_t, R_t, and R_0 from 91 various experiments with full thickness skin, isolated dermis, and hydrated dermis were introduced into Kottler's formulae to specify a mean value for r_i [Kottler, 1960]. This value was used in the following propagation model.

Optical Propagation Model

The one-dimensional (1-D) diffusion approximation solution to the transport equation [Ishimaru, 1978] provided a means 1) to compute the expected T_d and R_d, given a choice of s, k, and g, and 2) to compute the distribution of light within the tissue. An initial choice of s, k, and g, was made, and the expected T_d and R_d were calculated. Comparison with the observed T_d and R_d allowed an improved choice of s, k, and g. Iteration of this choice/comparison/improved choice algorithm converged quickly to a unique set of s, k, and g values. The choices of s and k always met the constraint that $s + k$ equaled γ, the attenuation constant for collimated light:

$$T_c = e^{-\gamma d} \quad \text{or} \quad \gamma = -\ell n(T_c)/d \qquad (5)$$

where d was the sample thickness in cm. The implementation of the 1-D solution is presented in Appendix I. In the appendix the absorption coefficient k is denoted $\rho\sigma_a$, the scattering coefficient s is denoted $p\sigma_s$, and the attenuation constant γ is denoted $p\sigma_t$, to be consistent with the notation of Ishimaru [1978].

Thermal Diffusion Model

The optical distribution obtained for the best choice of s, k, and g multiplied by the absorption coefficient, k, yielded the spatial distribution of photon deposition in W/cc, which is the distributed heat source for a thermal diffusion problem. A one-dimensional Green's function for thermal diffusion in a wet tissue was convolved against the spatial distribution of photon deposition within the tissue to yield the temperature distribution within the tissue as a function of time (see Appendix II). The Green's function was based on the following assumed values: 0.80 cal/g-°C for heat capacity, C, 1.09 g/cc for density, ρ, and 1.01 $\times$ 10^{-3} cm^2/s for diffusivity, α, which are all based on the expected values for a tissue with 70% water content, W, according to the review of Takata et al [1977; see Welch, 1984], and assuming a density of 1.3 g/cc for dry tissue:

$$\begin{aligned} C &= [0.37 + 0.67W/\rho](\text{cal/g}-^0\text{c}) \\ \alpha &= [0.133 + 1.36W/\rho) \times 10^{-3}] \ (\text{cm}^2/\text{s}) \qquad (6) \\ \rho &= [1.3 - 0.3W] \ (\text{g/cc}) \end{aligned}$$

Temperature Threshold for Thermal Coagulation

To determine the threshold temperature for tissue coagulation, three full thickness skin samples were each

marked with a 3 × 3 grid of black points separated 1 cm apart. The grid was easily documented by making a photocopy of the tissue sample held on the outer surface of a petri dish. The samples were immersed for 10 s in a well-stirred water bath at a known temperature, removed to the petri dish, and again photocopied. This procedure was repeated for increasing water bath temperatures. When the threshold temperature for coagulation was reached, the spacing between the grid points suddenly decreased. To determine the kinetics of coagulation, 18 skin samples from six mice were repeatedly immersed for 10-s periods in the water bath at one of three temperatures, 62°C, 64°C, or 66°C (six samples per temperature tested). The degree of coagulation in the direction of lateral orientation across the back of the mouse as a function of time was recorded.

Argon Laser Experiments

Three anesthetized animals (BALB/c mice, 6–8 weeks old, 0.8% chloral hydrate, 0.1 ml per 10 g body weight) were the subjects of argon laser irradiation at 488 nm wavelength. The ambient skin temperature was 29° ± 1°C, as measured by thermocouple. Laser light was transmitted through 4 feet of 600-μm diameter optical fiber, and focused through a ×10 objective lens to yield a 3-mm diameter image of the fiber tip on the animal's back. This method of optical delivery produced a very flat field. The irradiance of the spot could be adjusted up to 60 W/cm^2 by controlling the electrical discharge current in the laser. The laser light was delivered in either 1/2-s or 1-s pulses by a timed shutter at increasing irradiances until thermal coagulation of the skin was observed.

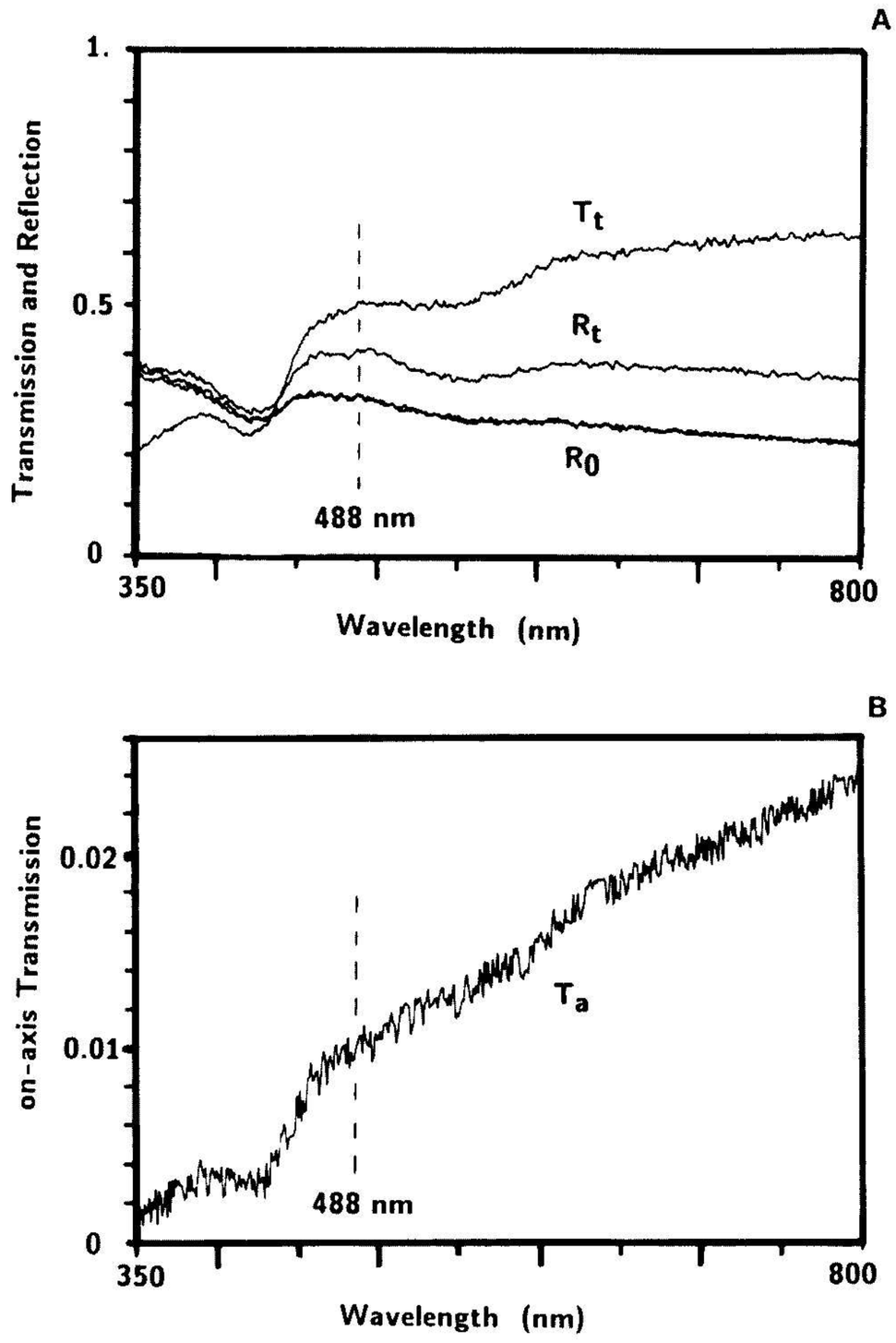

Fig. 2. The spectrophometric data from 350–800 nm for one of the mouse skin samples. **A**: The total transmission, T_t, the total reflection, R_t, and the total reflection with a black backing, R_0. Two R_0 scans are plotted, one for a black painted glass slide backing and the other for an India ink/agar backing, but they are indistinguishable. **B**: The on-axis transmission, T_a.

RESULTS

Optical Measurements

The total transmission, T_t, total reflection, R_t, and total reflection with a black backing, R_0, are shown in Figure 2A for wavelengths from to 350 to 800 nm, and the on-axis transmission, T_a, is shown in Figure 2B. At shorter wavelengths absorption was significant, and all measurements decreased. Some blood remained in this fresh tissue specimen, as indicated by absorption centered at 418 nm and 540–580 nm. At 488 nm there was only a slight contribution to the absorbance by the blood, and dermal absorbance was the dominant site of photon deposition. The following results consider only the data at 488 nm, as listed in Table I.

The calculated values for the intrinsic optical parameters, s, k, and g, based on the γ, T_t, and R_t values, are summarized in Table II. The ability to determine k was sensitive to thin spots in the dermis that occasionally occurred during preparation. The determination of s and g were less sensitive to such problems in technique.

To illustrate how the s, k and g parameters were calculated, Figure 3 plots as R_t versus T_t both the measured data and the expected values based on the different choices of s, k, and g. The graph is appropriate for a tissue thickness of 116 μm (average single skin thickness) and a wavelength of 488 nm. The grid is based on a γ value of 242 cm^{-1}, and shows constant g lines at various k and constant k lines at various g. The mouse skin values are those expected for a tissue that is 116 μm thick, according to Figure 4 (below). There is a unique choice for s, k, and g, which corresponds to mouse skin. The curve in the grid that corresponds to $g = 0$ indicates the behavior of purely isotropic scattering media. Mouse skin scatters light in a more strongly forward direction, which increases T_t and decreases R_t. (The negative reflec-

TABLE I. Summary of Measurements on Mouse Skin

No.	d	T_a	T_t	R_t	R_0
1	123	.0121	.525	.440	.283
2	161	.0198	.578	.341	.256
1 + 2	199	.0033	.360	.491	.438
3	80	.0546	.629	.241	.123
4	132	.0457	.6782	.229	.137
3 + 4	134	.0168	.567	.321	.170
5	101	.0257	.587	.281	.150
6	80	.0796	.713	.205	.094
5 + 6	164	.0123	.479	.338	.197
7	96	.1689	.689	.252	.125
8	100	.2307	.681	.254	.142
7 + 8	152	.0629	.591	.288	.176
9	118	.0703	.702	.234	.135
10	133	.0823	.687	.275	.150
9 + 10	211	.0189	.588	.347	.225
11	117	.0517	.648	.283	.175
12	119	.1673	.706	.224	.140
11 + 12	185	.0380	.585	.304	.228
13	126	.0311	.632	.274	.184
14	132	.0683	.726	.246	.123
13 + 14	232	.0087	.5038	.363	.253

No., specimen No. (double layers indicated by sum); d, tissue thickness (μm); T_a, on-axis transmission, within 4.4° half angle of acceptance; T_t, total transmission, collected by integrating sphere; R_t, total reflection, collected by integrating sphere; R_0, R_t for tissue with a black backing.

TABLE II. Summary of Calculated Intrinsic Optical Parameters

No.	s	k	g
1	361	1.1	.66
2	241	2.0	.74
1 + 2	298	3.0	.58
3	350	7.0	.78
4	228	2.9	.84
3 + 4	303	3.3	.76
5	354	5.3	.78
6	304	4.2	.84
5 + 6	264	4.7	.71
7	173	2.5	.67
8	135	2.7	.57
7 + 8	175	3.4	.69
9	218	1.4	.80
10	181	1.1	.75
9 + 10	187	1.2	.75
11	246	2.3	.76
12	141	2.4	.72
11 + 12	172	2.5	.72
13	270	3.0	.80
14	199	0.8	.82
13 + 14	206	2.3	.73
Mean	238	2.8	.74
SD	67	1.5	.07

No., specimen No. (double layers indicated by sum); s, scattering coefficient (cm^{-1}); k, absorption coefficient (cm^{-1}); g, anisotropy.

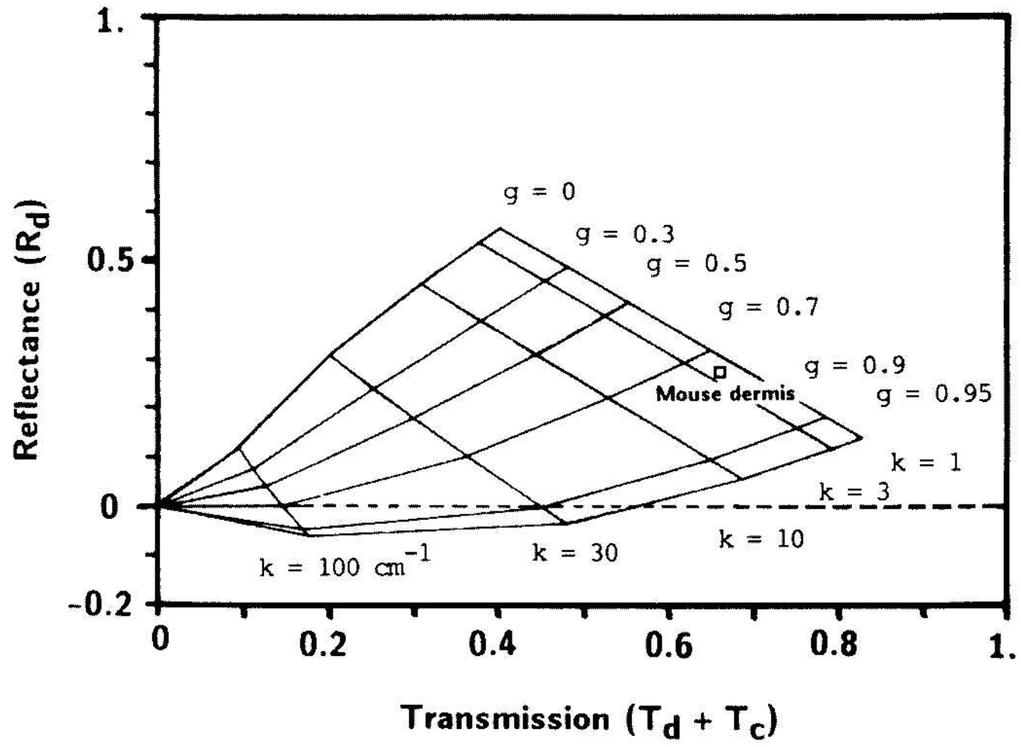

Fig. 3. Diffuse reflectance, R_d, versus diffuse plus collimated transmission ($T_d + T_c$) at 488 nm. The values for mouse skin expected for a 116-μm tissue thickness are mapped as a single point. The grid indicates the theoretical values for R_d and ($T_d + T_c$) for a range of values for absorption, k, scattering, s, and anisotropy, g. This grid meets the constraints: $k + s = 242$ cm^{-1}, and thickness, d, equals 116 μm, which was the average dermal thickness.

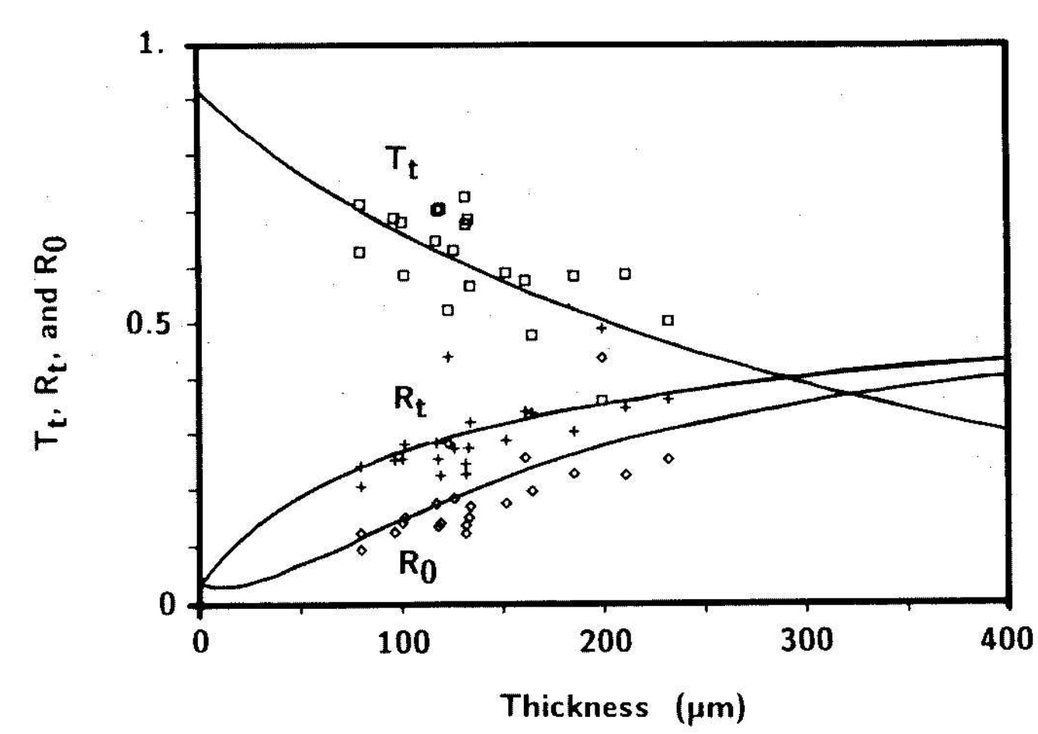

Fig. 4. The measurements on mouse skin at 488 nm, plotted as a function of sample thickness. The total transmission, T_t (□), total reflectance, R_t (+), and total reflectance with a black backing, R_0 (◇), are shown.

tance indicated by the grid for very anisotropic media [g close to 1] are expected. The diffusion approximation assumes that light distribution is nearly uniform. For highly anisotropic media, the boundary conditions cannot satisfy the constraints that light be both nearly uniform and highly anisotropic, and the model breaks down.)

The measured values for T_t, R_t, and R_0 are plotted in Figure 4 as a function of sample thickness, d. The theoretical curves for T_t, R_t, and R_0, as calculated by the 1-D model, using the average values for s, k, and g in

Table II are plotted as solid lines. To compute R_0, the internal reflection, R_i, at the inner boundary was set to equal zero. The black backing during the R_0 measurement absorbed any light that reached the back of the tissue, and decreased the observed R_t since there was no longer internal reflectance at the back interface. There was no difference in R_0 measurements made with a black painted glass slide versus an agar gel containing India ink. Since the R_0 measurements were not used to deduce the s, k, and g values, the agreement of the theoretical curve and the observed R_0 data constitutes a test of the predictive ability of the model.

Predicted Optical and Thermal Distributions In Vivo

The distributions of optical fluxes in vivo as calculated by the 1-D model using the average values of s, k, and g in Table II are plotted in Figure 5. The internal reflectance from the inner skin surface was assumed to be zero, which was an approximation since there was actually some reflectance from the deeper tissues. The incident collimated flux, C, attenuated quickly, and the $1/e$ depth equaled 40 μm. The forward diffuse flux, I, increased to a maximum near an 80-μm depth. The backward diffuse flux, J, increased steadily toward the tissue front surface. The total effective flux, F_{eff} in W/cm^2, which contributed to heating, equaled $C + 2(I + J)$. (See Appendix I.) F_{eff} achieved a maximum value at a depth of 45 μm that was more than twice the incident collimated flux, F_0. At the surface, F_{eff} exceeded F_0 by 52%. (F_0 equal to 55 W/cm^2.)

The distribution of temperature in vivo during argon laser irradiation was calculated (see Appendix II) based on the predicted optical flux distribution in Figure 5A. The temperatures at 0.5, 1, 2, 3, 5, and 9 s of laser irradiation are plotted in Figure 5B. Thermal diffusion distributed the absorbed laser energy, and a subsurface maximum in temperature was not obvious. The dermis was relatively evenly heated to 70°C by 2 s of laser irradiation. After 5–9 s of irradiation, temperatures were in the neighborhood of 100–120°C.

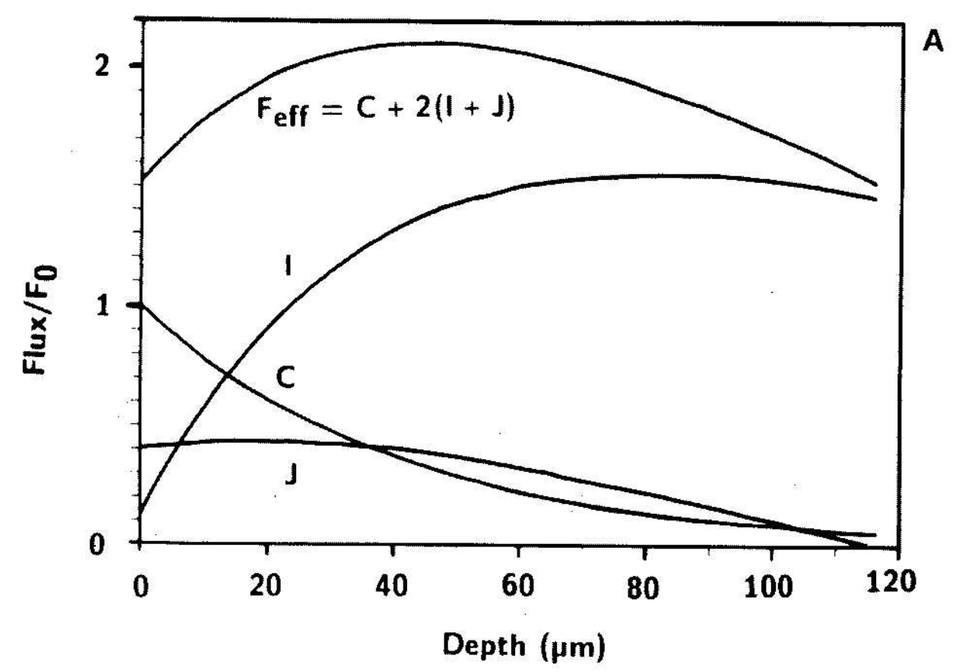

Fig. 5. The calculated distribution of optical fluxes and temperatures within mouse skin during argon laser irradiation. **A**: The collimated flux, C, the forward diffuse flux, I, the backward diffuse flux, J, and the total effective flux, $F_{eff} = C + 2(I + J)$, which contributes to heating. **B**: The calculated distribution of temperatures versus tissue depth during argon laser irradiation in vivo at 55 W/cm^2. The temperature profiles at 0.5, 1, 2, 3, 5, and 9 s are shown. Initial skin temperature was 29°C.

Thermal Coagulation

Coagulation of in vitro skin occurred above 60°C, as indicated by the contraction of the tissue and as documented by the decrease in grid spacing. The kinetics of coagulation were first order, as shown in Figure 6 in which the grid spacing, x, in cm is plotted versus time of

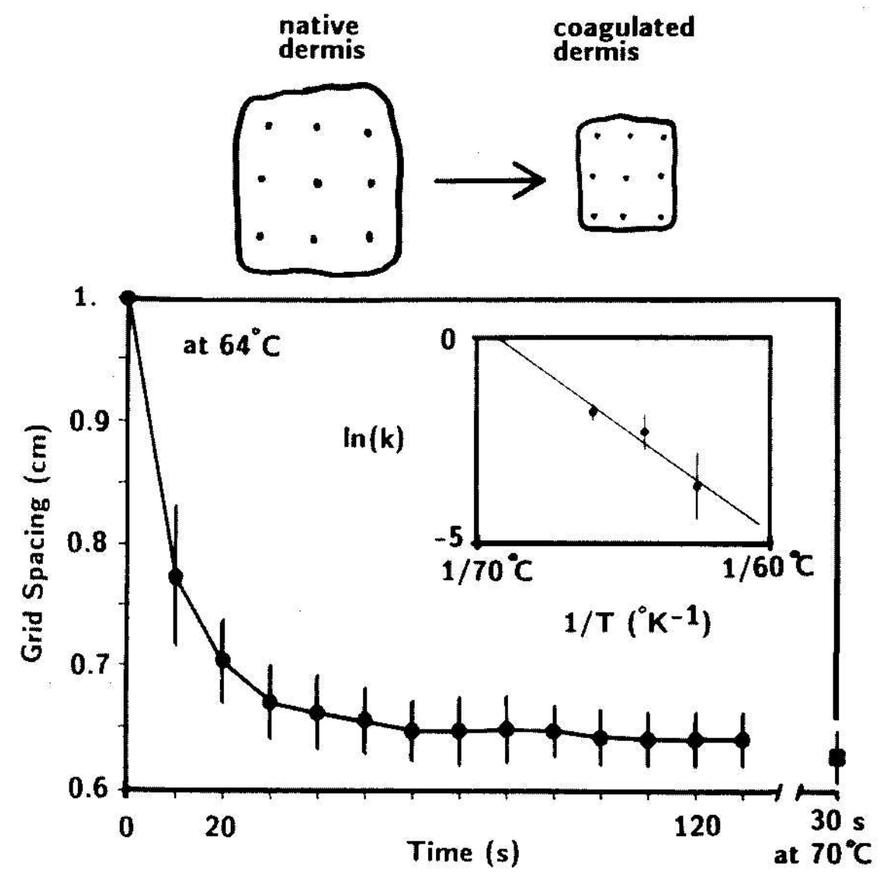

Fig. 6. The thermal coagulation of mouse skin at 64°C. The spacing between grid points drawn on a skin sample decreased with repeated 10-s immersions. The mean grid spacing for six specimens is plotted versus accumulated time of immersion, and standard deviations are shown. **Insert**: the first order rate constants, k (s^{-1}), for coagulation at 62°C, 64°C, and 66°C are plotted versus inverse temperature. The slope yields a molar enthalpy of 102 kcal/mol and the y-intercept at infinite temperature yields a molar entropy of 296 cal/mol-°K.

immersion, t. The grid spacing decreased with time of immersion:

$$x = [1 - (1 - x_{max})(1 - e^{-kt})] \text{ (cm)} \quad (7)$$

where x_{max} is the grid spacing after maximum coagulation, and k is a first-order rate constant, in s^{-1}. The same x_{max} was achieved after several repeated exposures at 62, 64, or 66°C. Subsequent 30-s exposure to a 70°C bath did not cause significant further coagulation. Table III summarizes the data. The rate constant, k (s^{-1}), increased with temperature according to an Arrhenius relationship (see insert, Fig. 6):

$$\ell n(k) = \Delta S/R + \Delta H/RT \quad (8)$$

where molar entropy, ΔS, equaled 297 cal/mol-°K and molar enthalpy, ΔH, equaled 102 kcal/mol.

Experimental Argon Laser Photocoagulation

The threshold for photocoagulation of mouse skin in vivo by CW argon laser irradiation was a 1.5-s pulse at 55 W/cm^2, which produced a whitening of the skin owing to the increased scattering of coagulated dermis. A 2-s pulse at this irradiance reliably achieved coagulation. Obvious contraction of the skin site began at this time. If the laser irradiation was delivered continuously, a sudden explosive vaporization occurred at 5–10 s, which according to Figure 5b was when temperatures exceeded 100°C. Onset of this explosive event was variable.

DISCUSSION

This method for experimental specification of the intrinsic transport parameters for a tissue is appropriate for thin specimens. It is necessary for sufficient light to penetrate the specimen so that a reliable measurement of T_a is made. The acceptance angle for the T_a measurement on this spectrophotometer was ±4.4°. There is a degree of arbitrariness and oversimplification in choosing to call light accepted within this angle "on-axis," and to call all transmitted light not collected "diffuse." A laser beam does not immediately become "diffuse" after a single scattering event, according to goniometric studies of the angular dependence of dermal scattering (S. Jacques, unpublished study). How different would the calculated s, k, and g values be if a spectrophotometer with a larger or smaller acceptance angle was used? The limits of this approach toward specification of tissue optical parameters are currently under study. However, at this time we feel that these concerns will not prove serious, and the method offers a simple approach using equipment widely available.

The optical distribution within the tissue showed a maximum total flux at a depth of 45 μm beneath the skin surface. However, the thermal diffusion throughout the dermal thickness of 116 μm was rapid, and the temperature distribution was quite even. Such uniform heating can achieve a controlled coagulation, which offers a reliable wound model for tissue-response studies.

The kinetics of coagulation are temperature dependent. The rate constant becomes very slow below 60°C and very fast above 70°C. Within this threshold temperature range the coagulation process takes seconds, and there is ample opportunity for changes in optical properties to occur, which would alter the photon deposition. For example, a recent report describes how thermal coagulation affects the optical properties of aorta by doubling reflectance and halving transmission [Gourgouliatos et al, 1986]. Work continues on the optical changes that occur during dermal coagulation and on how to incorporate such changes into the simulation of laser irradiation of tissue.

TABLE III. Thermal Coagulation of Mouse Skin

T	x_{max}	$x_{70°}$	k
62°C			
Average	.648	.638	.036
SD	.045	.022	.026
64°C			
Average	.645	.628	.109
SD	.025	.026	.037
66°C			
Average	.661	.635	.116
SD	.064	.041	.037

Six samples at each temperature (three samples per mouse).
T, water bath temperature (°C); x_{max}, grid spacing after maximum coagulation (cm); $x_{70°}$, grid spacing after 30 s at 70°C (cm); k, first-order rate constant (s^{-1}).

ACKNOWLEDGMENTS

We thank Martin van Gemert, Willem Star, Wai Fung Cheong, Norm Nishioka, and Rox Anderson for many important discussions; A.J. Welch and John Parrish for their interest and facilitation in the collaboration of our laboratories; Rick Granstein for help with the in vivo argon irradiation experiments; Susan Clegg for help with the optical measurements; and Kosta Zinis for help with the in vitro thermal coagulation experiments. The latter three persons continue in the mouse skin studies, which will be reported in more complete form.

This work was supported by NIH grant AM25395-08, O.N.R. Contract #N001486K0017, and the Arthur O. and Gullan M. Wellman Foundation.

REFERENCES

Abramowitz M, Stegun IA, eds.: "Handbook of Mathematical Functions." eq. 7.4.32, New York: Dover Publications Inc., 1972, p 303.

Bausch and Lomb: "Refractive Index and Percent Dissolved Solids Scale." Analytic Systems Division (S-5195 0675).

Birngruber R: Thermal modeling in biological tissues. In Hillenkamp F, Pratesi R, Sacchi CA (eds): "Lasers in Biology and Medicine." New York and London: Plenum Press, 1980.

Carslaw HS, Jaeger JC: "Conduction of Heat in Solids." Oxford: Clarendon Press, 1973.

Gourgouliatos ZF, Welch AJ, van Gemert MCJ: Behavior of optical properties of tissue (transmittance and reflectance) as a function of temperature (abstract). Lasers Surg Med 6:166, 1986.

Groenhuis RAJ, Ferwerda HA, Ten Bosch JJ: Scattering and absorption of turbid materials determined from reflection measurements. Applied Optics 22:2456–2462, 1983.

Ishimaru A: "Wave Propagation and Scattering in Random Media." New York: Academic Press, 1978.

Kottler F: Turbid media with plane-parallel surfaces. J Optical Soc 50:483–490, 1960.

Sliney D, Wolbarsht M: "Safety with Lasers and Other Optical Sources: A comprehensive handbook." New York: Plenum Press, 1980, p 22.

Solan JL, Laden K: Factors affecting the penetration of light through stratum corneum. J Soc Cosmet Chem 28:125–137, 1977.

Takata AN, Zaneveld L, Richter W: Laser-induced thermal damage in skin. USAF School of Aerospace Med., Brooks AFB, TX, Rep. SAM-TR-77-38, 1977.

Welch AJ: The thermal response of laser irradiated tissue. IEEE J Quantum Electronics QE-20:1471–1481, 1984.

APPENDIX I. One Dimensional Optical Propagation

The transport equation with no internal sources is (the notation and derivation in this appendix closely follow that by Ishimaru [1978]):

$$\boldsymbol{s}\cdot\nabla I(\boldsymbol{r},\boldsymbol{s}) = -\rho\sigma_t I(\boldsymbol{r},\boldsymbol{s}) + \frac{\rho\sigma_t}{4\pi}\int_{4\pi} p(\boldsymbol{s},\boldsymbol{s}')\, I(\boldsymbol{r},\boldsymbol{s}')\, d\omega'$$

where $I(\boldsymbol{r},\boldsymbol{s})$ is the total specific intensity ($W/cm^2/sr$) at position $\boldsymbol{r}$ in the direction of the unit vector $\boldsymbol{s}$ and $d\omega'$ is the differential solid angle in the direction $\boldsymbol{s}'$. The total scattering coefficient $\rho\sigma_t$ is the sum of the absorption and scattering coefficients, which are denoted by $\rho\sigma_a$ and $\rho\sigma_s$, respectively. The phase function $p(\boldsymbol{s},\boldsymbol{s}')$ represents the fraction of light scattered from the direction $\boldsymbol{s}$ into the direction $\boldsymbol{s}'$.

The total intensity $I(\boldsymbol{r},\boldsymbol{s})$ is split into collimated $I_{ri}(\boldsymbol{r})$ and diffuse $I_d(\boldsymbol{r},\boldsymbol{s})$ portions.

$$I(\boldsymbol{r},\boldsymbol{s}) = I_{ri}(\boldsymbol{r}) + I_d(\boldsymbol{r},\boldsymbol{s})$$

Assuming that the collimated beam is uniform and normal to the surface of the slab, then

$$I_{ri}(\boldsymbol{r}) = F_0\, e^{-\rho\sigma_t z}\, \delta(\omega_s\cdot\omega_z)$$

where z is a unit vector in the direction of increasing z (normal and into the slab). F_0 has units of W/cm^2 and $\delta(\omega_s\cdot\omega_z)$ is a solid angle delta function with units of sr^{-1}.

The diffusion approximation expresses the diffuse intensity as the sum of an isotropic part $U_d(\boldsymbol{r})$ and an anisotropic part $\boldsymbol{F}_d(\boldsymbol{r})\cdot\boldsymbol{s}$:

$$I_d(\boldsymbol{r},\boldsymbol{s}) = U_d(\boldsymbol{r}) + \frac{3}{4\pi}\boldsymbol{F}_d(\boldsymbol{r})\cdot\boldsymbol{s}$$

where

$$U_d(\boldsymbol{r}) = \frac{1}{4\pi}\int_{4\pi} I_d(\boldsymbol{r},\boldsymbol{s})\, d\omega,\quad \boldsymbol{F}_d(\boldsymbol{r}) = \int_{4\pi} I_d(\boldsymbol{r},\boldsymbol{s})(\mathrm{S}\cdot\mathrm{Z})\, d\omega.$$

In a slab of infinite extent in the x and y directions, the specific intensity cannot depend on x or y (for symmetry reasons). By making the above substitutions the transport equation reduces to the photon diffusion equation,

$$\frac{d^2U_d(z)}{dz^2} - \kappa_d{}^2 U_d(z) = -\mathrm{Q}_0\, e^{-\rho\sigma_t z} \qquad \text{(A1)}$$

where $\rho\sigma_{tr} = \rho\sigma_s(1-g) + \rho\sigma_a$ is the transport coefficient, $Q_0 = (3/4\pi)F_0(\rho\sigma_s\rho\sigma_{tr} + \rho\sigma_s\rho\sigma_t\mathrm{g})$,and $\kappa_d{}^2 = 3\rho\sigma_a\rho\sigma_{tr}$. The anisotropy coefficient g (equivalent to the $\bar{\mu}$ of Ishimaru) is defined as the average cosine of the phase function

$$g = \frac{1}{4\pi\omega_0}\int_{4\pi} p(\boldsymbol{s}',\boldsymbol{s})\,(\boldsymbol{s}\cdot\boldsymbol{s}')\, d\omega,\quad \text{where } \omega_0 = \frac{\rho\sigma_s}{\rho\sigma_t}$$

The treatment of boundary conditions follows Groenhuis et al [1983] who assumed that the diffuse flux moving in the Z direction downward from the top surface was equal to the reflection of diffuse flux moving upward. Thus, if $\mu = \boldsymbol{s}\cdot\boldsymbol{z}$ and r_i is the internal reflection coefficient, then at the top surface

$$\int_{2\pi} I_d(\boldsymbol{r},\boldsymbol{s})\,(\boldsymbol{s}\cdot\boldsymbol{z})\, d\omega = r_i \int_{2\pi} I_d(\boldsymbol{r},\boldsymbol{s})\,(\boldsymbol{s}\cdot\boldsymbol{z})\, d\omega,$$
$$\mu>0 \qquad\qquad \mu<0$$

which reduces to the mixed inhomogeneous boundary condition

$$U_d(z) - h'\frac{dU_d(z)}{dz} + \frac{Q_1'(z)}{2\pi} = 0;\ @\ z = 0. \qquad \text{(A2.1)}$$

A similar boundary condition is found for the bottom surface,

$$U_d(z) + h'\frac{dU_d(z)}{dz} - \frac{Q_1'(z)}{2\pi} = 0;\ @\ z = d, \qquad \text{(A2.2)}$$

where

$$h' = \frac{1 + r_i}{1 - r_i} \cdot \frac{2}{3\rho\sigma_{tr}} \text{ and } Q_1'(z) = \frac{1 + r_i}{1 - r_i} \cdot \frac{g\rho\sigma_s F_0}{\rho\sigma_{tr}} e^{-\rho\sigma_{tr}z}.$$

The r_i used to calculate h' in A2.1 (top surface) may be chosen to be different than the r_i used for h' in A2.2 (bottom surface).

Solutions to (A1) subject to boundary conditions (A2) are given by Ishimaru, except that his $Q_1(z)$ and h are replaced by $Q_1'(z)$ and h'.

$$U_d(z) = Ae^{-\rho\sigma_t z} + C_1 e^{\kappa_d z} + C_2 e^{-\kappa_d z} \quad \text{(A3)}$$

where $A = -Q_0/[(\rho\sigma_t)^2 - \kappa_d{}^2]$. C_1 and C_2 can be found by substituting (A3) into (A2) and solving the resulting pair of linear simultaneous equations for C_1 and C_2:

$$C_1(1 - h'\kappa_d) + C_2(1 + h'\kappa_d) = -A(1 + \rho\sigma_t h') - (1/2\pi)Q_1'(0),$$

$$C_1(1 + h'\kappa_d)e^{\kappa_d d} + C_2(1 - h'\kappa_d)e^{-\kappa_d d} = -A(1 - \rho\sigma_t h')e^{-\rho\sigma_t d} + (1/2\pi)Q_1'(d).$$

Once C_1 and C_2 are known, then $U_d(z)$ may be calculated from (A3). The total intensity (W/cm^2) at a depth z is given by

$$I_{total}(z) = 4\pi U_d(z) + F_0 e^{-\rho\sigma_t z}. \quad \text{(A4)}$$

The product of the absorption coefficient $\rho\sigma_a$ and $I_{total}(z)$ yields the photon deposition in W/cc.

The distribution of light may also be discussed in terms of the collimated, forward diffuse, and backward diffuse fluxes, C, I, and J, respectively, which are expressed in W/cm^2 rather than the units W/cm^2-sr that are used for U_d. The definitions of these fluxes are given:

$$C = F_0 e^{-\rho\sigma_t z}$$

$$I = 2\pi(U_d/2 + B)$$

$$J = 2\pi(U_d/2 - B)$$

where

$$B = h(-\rho\sigma_t A e^{-\rho\sigma_t z} + \kappa_d[C_1 e^{\kappa_d z} - C_2 e^{-\kappa_d z}])/2$$

The total effective flux, F_{eff} in W/cm^2, which contributes to heating, equals $C + 2(I + J)$, and is identical to I_{total} given in (A4). The factor of 2 accounts for the average double pathlength traveled by diffuse light compared to collimated light.

The diffuse transmission and reflection are given:

$$T_d = \mathrm{I}(z = d)/\mathrm{F}_0 \quad \text{(A5)}$$
$$R_d = \mathrm{J}(z = 0)/\mathrm{F}_0$$

Finally, the experimentally observed T_t and R_t values are given:

$$T_t = (1 - R_{s1})[T_d + (1 - R_{s2})T_c] \quad \text{(A6)}$$
$$R_t = R_{s1} + (1 - R_{s1})R_d$$

where R_{s1} and R_{s2} are the specular reflectances at the front and back surfaces, respectively, of the tissue sample, and T_c is the collimated transmission equal to $F_0 e^{-\rho\sigma_t d}$.

The implementation of the inverse model (model^{-1}) iteratively compared predicted T_d and R_d values (A5) that were based on choices of $\rho\sigma_a$, $\rho\sigma_s$, and g, with experimental T_d and R_d values, that were calculated from T_t, R_t, and T_c by rearrangement of (A6). The algorithm efficiently converged on a unique set of intrinsic optical properties for each tissue sample.

APPENDIX II. One-Dimensional Thermal Diffusion

The process of thermal diffusion obeys the relation [Carslaw and Jaeger, 1973; Birngruber, 1980]:

$$\rho C dT/dt = q + \alpha\nabla^2 T \quad \text{(A7)}$$

where ρ is the tissue density (g/cc), C is the specific heat (J/g-°C), α is the thermal diffusivity (J/cm-s-°C), q is the rate of deposition of photon energy (J/cc-s), T is temperature, and t is time (s). This relation neglects the influence of blood flow, metabolic heat generation, surface water evaporation, and convection, which are important for CW laser irradiation but not for laser pulses of only a few seconds in duration. The one-dimensional impulse response solution to equation 7 for an impulse of heat, Q in joules, deposited at time t' and position x', is given:

$$T_0(x,t) = \frac{Q}{2\rho C[\pi\alpha(t - t']\frac{1}{2}} e^{-(x-x')^2/4\alpha(t-t')} \quad \text{(A8)}$$

The convolution of this impulse response over both the spatial and temporal distribution of the photon energy deposition yields the temperature at a given position, x, and time, t:

$$T(x,t) = [1/\rho C(\pi\alpha)^{1/2}] \int_0^t \int_{-\infty}^{+\infty} [q(x',t')/(t-t')^{1/2}] e^{-(x-x')^2/4\alpha(t-t')}\, dx'dt' \quad (9)$$

where $q(x',t')$ represents the rate of photon energy deposition as a function of time and depth within the tissue and can specify any temporal history of irradiation and spatial distribution of photon absorption by the tissue. The optical model (Appendix I) specified the photon deposition, $\rho\sigma_a I_{total}$, which yielded a $q(x')$ for a unity (1 J/cm^2) incident flux, independent of time. In our experiments, the laser output was a step function of magnitude 55 J/cm^2-s; therefore $q(x't')$ was given by the product $55q(x')$ in J/cm^2-s.

Equation A9 is a general description of the 1-D heat flow process, based on the impulse response to a Dirac delta function. During implementation on the computer, a square pulse function of arbitrarily small width replaced the delta function, to yield a "square pulse" response efficiently evaluated [Abramowitz and Stegun, 1972]:

$$T_0(x,t) = (Q/2\rho C)(\pi/a)^{1/2}[erf(a^{1/2}r) - erf(a^{1/2}r)] \quad \text{(A10)}$$

where a equals $(4\alpha t)^{-1/2}$, and r is the radius of the square pulse, which was set to 0.5 μm in this case since the tissue model was composed of 1-μm-wide elements for calculations. The *erf* function was evaluated by reference to a table held in the computer.

The continuous laser irradiation was treated as a series of impulses spaced at 1-ms intervals, each having an energy $Q(x)$ equal to (55 J/cm^2-s)(1 ms), or 55 mJ/cm^2, and calculations were made in time steps of 1 ms. The choice of interval was arbitrary, based on the resolution desired, and can be as short as required in other problems. At each time step, the square pulse response (eq. A10) was evaluated for time t and for all distances, $x - x'$, from a source, and the results were stored in an array for efficient access. Then, the contributions of heat to a given element from all other elements were calculated:

$$\text{heat contribution} = \sum_{x'} Q(x',t)T_0(|x-x'|,t) \quad \text{(A11)}$$

As t increased with each time step, the contribution from heat flow finally arriving at time t at a given element was added to the accumulated heat content of that element. This accumulation constituted the time integral of equation A9, and equation A11 constituted the spatial integral of equation A9. Once laser irradiation was halted, the time-consuming time steps on the computer were no longer necessary. Equation A11 could yield the heat distribution at any later time by a single calculation.

The air/skin interface constituted an insulating boundary, and any heat flow to the surface was reflected back into the tissue. The mirror image of the heat source term $q(x')$ was extended into the air space above the skin, and heat was considered to flow from this image tissue. This mirror image technique properly solved the insulating boundary problem.